Investigation of active tracking for robotic arm assisted magnetic resonance guided focused ultrasound ablation

Xiao, Xu; Huang, Zhihong; Rube, Martin A.; Melzer, Andreas

Published in:
International Journal of Medical Robotics and Computer Assisted Surgery

DOI:
10.1002/rcs.1768

Publication date:
2017

Licence:
Other

Document Version
Publisher's PDF, also known as Version of record

The International Journal of **Medical Robotics** and **Computer Assisted Surgery**

THE INTERNATIONAL JOURNAL OF MEDICAL ROBOTICS AND COMPUTER ASSISTED SURGERY
Int J Med Robotics Comput Assist Surg 2016.
Published online in Wiley Online Library (wileyonlinelibrary.com) **DOI:** 10.1002/rcs.1768

ORIGINAL ARTICLE

Investigation of active tracking for robotic arm assisted magnetic resonance guided focused ultrasound ablation

Xu Xiao[1]*
Zhihong Huang[2]
Martin A. Rube[1]
Andreas Melzer[1]

[1]*Institute for Medical Science and Technology, University of Dundee, Dundee, UK*

[2]*School of Engineering, Physics and Mathematics, University of Dundee, Dundee, UK*

*Correspondence to: Xu Xiao, Institute for Medical Science and Technology, University of Dundee, Wilson House, 1 Wurzburg Loan, Dundee Medipark, Dundee DD2 1FD, UK.
E-mail: XXiao@dundee.ac.uk

The work should be distributed to Institute for Medical Science and Technology. Sources of financial support: China Scholarship Council (CSC); European Union's Seventh Framework Programme under grant agreement no. 270186 (FUSIMO project) and no. 611963 (FUTURA project).

Accepted: 20 July 2016

Abstract

Background Focused ultrasound surgery (FUS) is a technique that does not need invasive access to the patient while allowing precise targeted therapy. Magnetic resonance (MR) guided FUS provides capabilities for monitoring treatments. Because the targeted tumours are distributed at different positions, focus repositioning becomes necessary.

Methods An MR compatible robot was used to increase the operational range of FUS application. Active tracking was developed to detect the robotic arm with regard to the MR coordinate system. The purpose of this study was to construct active tracking to allow a wide spatial range of repositioning the FUS transducer that is fast and accurate. The technique was characterised and validated by a series of positioning tests to prove its efficiency for guiding the robot.

Results In the calibration range, tracking achieved an RMS accuracy of 0.63 mm. Results of phantom ablation showed a focal scanning precision $\Delta x = 0.4 \pm 0.37$ mm, $\Delta y = 0.4 \pm 0.28$ mm and $\Delta z = 0.7 \pm 0.66$ mm.

Conclusions The active tracking localisation can be considered a feasible approach for the MR guided FUS system positioned by a robot. Copyright © 2016 John Wiley & Sons, Ltd.

Keywords active tracking; MR compatible robotic arm; MRI; focused ultrasound; MRgFUS

Introduction

Focused ultrasound (FUS) or high intensity focused ultrasound (HIFU), allows non-invasive tissue heating and ablation deep inside the body. An HIFU transducer is capable of converging ultrasonic pressure waves to a focal point on the scale of approximately 1 mm^3 inside living tissues without physical penetration (1). Sufficiently high energy of the incident ultrasound beam is able to produce clinically significant heating at the ultrasonic focus to induce subsequent local tissue necrosis. Heating along the ultrasonic beam path is usually negligible, but depends on tissues in the beam path and behind the focal spot.

MRI is a widely used tool to guide and monitor FUS therapy and improves safety, focal precision and energy deposition efficiency (2). MRI offers a high soft tissue contrast, which allows precise targeting and non-invasive temperature monitoring based on temperature-sensitive MR parameters such as the proton resonance frequency (3). Various clinical studies have been investigated for MRgFUS, e.g. breast tumours, bone metastases, uterine fibroids (4–6), and brain application (7–9), and most have received the CE mark and FDA approval.

To design an FUS therapy unit, patient access and MRI imaging compatibility have to be considered. Most of the MRgFUS systems are typically mounted onto or integrated into the patient table of the MR scanner to avoid interaction with the MRI bore (10), e.g. the Exablate 2000 Body System (InSightec, Ltd, Tirat Carmel, Israel) or Sonalleve (Philips, Vantaa, Finland).

During a typical FUS treatment process, multiple small foci of single ultrasonic exposures are combined to form a larger ablation zone until the entire target volume is covered. A complete FUS intervention requires a series of sonications and focus repositioning. For any clinical FUS applications, precise repositioning of the ultrasound focus is to be emphasised. Precise repositioning of the ultrasound focus guarantees complete tumour ablation and avoids damage to healthy tissue such as glands, nerves and blood vessels. Such a focal spot scanning technique can be realised mechanically via repositioning of transducers by robotic actuators or via electronic steering of the focal spot with phased-array transducers. Robotic positioning allows a wider spatial range and more flexible treatment access than electronic steering of phased-array transducers.

The proposed work focuses mainly on using an MR compatible robotic arm (11) to guide a custom-made fixed focused transducer for FUS treatment. With this setup, we aim to provide wider treatment access for mechanically assisted MR guided FUS treatment. With this robotic arm setup, the treatment could be conducted from above the patient. This will be a supplement to a traditional treatment method (Exablate 2000 body system), which could apply the sonication only from underneath the patient.

Furthermore, to maximise the benefits of the robotic arm system, we introduced the active tracking method to register the robotic arm into the MR space for a more automated guidance system. Registration methods for medical devices within the MR scanner coordinate system can be divided into two main categories – passive and active methods. The passive tracking of a medical device is based on passive contrast (12) markers. The original registration method of the INNOMOTION robotic arm uses passive contrast agent filled markers. These passive markers are used flexibly and especially safe for localisation of endorectal prostate biopsy (13) or other catheter interventions; this is because they do not involve any connecting wires or related tissue heating risks (14) during MRI. However, the localisation usually employs a more complex analysis of the image data (15), which makes this passive tracking approach relatively time consuming and susceptible to signal-to-noise ratio (SNR) of MR scans. Active tracking is based on resonance radiofrequency (RF) coils (16,17) with wireless inductive coupling with an MR imaging system (18). The position of the resonance coils can be measured by a dedicated MR pulse sequence that uses one-dimensional projections (19). Active tracking coils benefit medical devices because of their high accuracy and fast position updates, although their applications are restricted by the number of MR receiver channels and potential safety hazards due to the long conducting wires that connect the coil and the receiver of the MRI scanner. Considering that the goal of the present work was to optimise the combination of MR robotics and an MRgFUS system, active tracking by RF coils was chosen as the method for guiding the robotic arm.

The purpose of this study was to construct active tracking to allow a wide spatial range of repositioning the FUS transducer that is fast and accurate. The original registration method for the robotic arm is described and compared with the new method. The basic rationale of active tracking as well as the novel integration of active tracking and the calibration method for the robotic system are presented. We used low flip angle radiofrequency excitation pulses and projection readouts to localize the micro-resonance coil during MRI (20). This concept has been integrated into a dedicated non-imaging MR pulse sequence. Our tracking sequence employed weakly spatially-selective radiofrequency excitation pulses. And we used spoiling gradients at the end of each repetition to dephase the magnetisation and thus reduce phase coherences. This work serves as a preclinical feasibility study of MRI guided FUS application on phantoms with robotic assistance in a clinical 1.5 T MRI scanner.

Material and methods

Robotic arm with passive tracking

The robotic arm INNOMTION (IBSmm, Brno Czech Republic) that was used for this study is a pneumatically driven system with five degrees of freedom (DOF), which can be controlled to move over a translational range of ± 50 cm, while at a rotation of $\pm 40°$ in transverse and $-23°/+70°$ in the sagittal direction (Figure 1). The accessible space range could cover the whole field of view

DOI: 10.1002/rcs

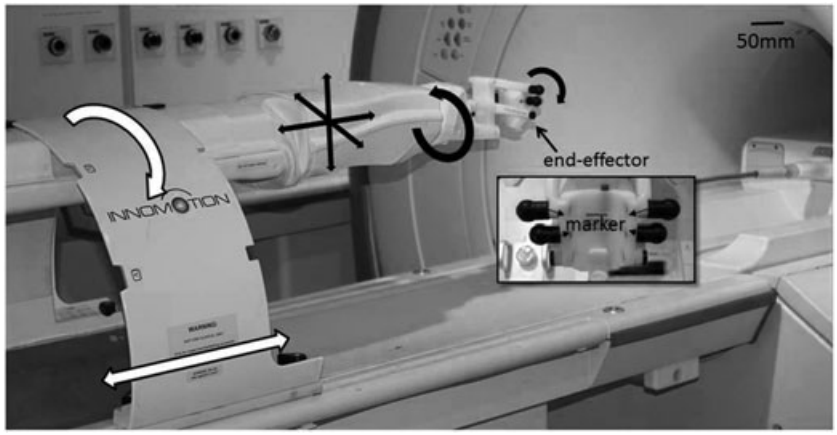

Figure 1. Photo of the robotic arm in front of a 1.5 T MRI scanner, the robot has 5 automate DOF (black arrows) and two manual DOF (white arrows). The enlarged end-effector is with four passive markers filled with Gadolinium contrast agent. Their positions are calculated via processing MR scans through these markers.

(FOV) of the clinical 1.5 T MRI scanner (Signa HDxt, GE Medical Systems, Waukesha, WI, USA). A previous study demonstrated that the robotic system can achieve an overall positioning accuracy of ±1 mm in translational direction and ±1° in angular direction respectively, which correlates with the specifications of the manufacturer (11,21).

The robotic arm is referenced with the coordinate system of the MR scanner using four spherical passive markers at the end-effector. A specific MR sequence, three-dimensional gradient echo (time of repetition: 150, time of echo: 30, flip angle 60), is applied on the markers, and the position of the markers in the image space is computed via extracting their centres by means of image processing algorithms (11). In addition to the long time, this approach requires a prior knowledge of rough position information of the markers in order to select the appropriate scan planes and to detect the markers.

Active tracking of the robotic system

To speed up the registration of the robotic arm in the MR frame reference, micro-resonance coils (mRC) (19) are used to replace the passive markers on the application module.

The mRC was designed as a spiral coil 2 mm in diameter and 5 mm in length (Figure 2). The solenoid coil with seven to eight winding loops includes a small volume of 100:1 aqueous gadolinium contrast agent solution with a size of approximately 2 mm in diameter and 10 mm in length. The mRC was tuned in air to f0 = 63.8 MHz, the proton Larmor frequency at 1.5 T, using an RF impedance analyzer (Agilent4191A, Agilent, Santa Clara, United States).

Since the mRCs are tuned to resonate at the proton Larmor frequency of the MRI system (22), according to the principle of electromagnetic induction, radiofrequency (RF) pulses with low Flip Angle (FA) lead to substantial rotation of magnetization within the central flux of the coil (22). And the solution of gadolinium contrast agent with short T1 within the mRC will enhance this effect.

We used low FA RF excitation pulses and projection readouts to localize the mRC during MRI (20). This concept has been integrated into a dedicated non-imaging MR pulse sequence proposed by Dumoulin (23). The difference is that our tracking sequence employed weakly-spatially-selective RF excitation pulses, rather than active tracking pulse sequences, with low FA. And we used spoiling gradients at the end of each repetition to dephase the magnetization and thus reduce phase coherences.

The pulse sequence diagram is shown in Figure 3. The readout scheme could provide 3D positional information within four excitations. Thus, the implementation required four times the number of different dephasing gradient directions ($N \times 4 \times TR$) to compute the position of the mRC. To improve the SNR, we used six phase-field dithering directions for every repetition (23), which resulted in a tracking duration of $6 \times 4 \times TR$ (120 ms, N = 6, TR = 5 ms). Thus, the tracking rate can be as high as 8.3 frames per second.

The coil of the mRC has all dimensions matching the readout resolution. This resulted in sharp peaks (Figure 3(b)) in the power spectrum whose frequency is indicative of the location of the mRC along respective dimensions. The tracking sequence was implemented with standard multiple receiver imaging coils and no limitation of receiver channels. The tracking pulse sequence parameters were used as follows: TE = 1.52 ms, TR = 2.18 ms, FA = 0.3°, FOV = 48 cm along the readout

DOI: 10.1002/rcs

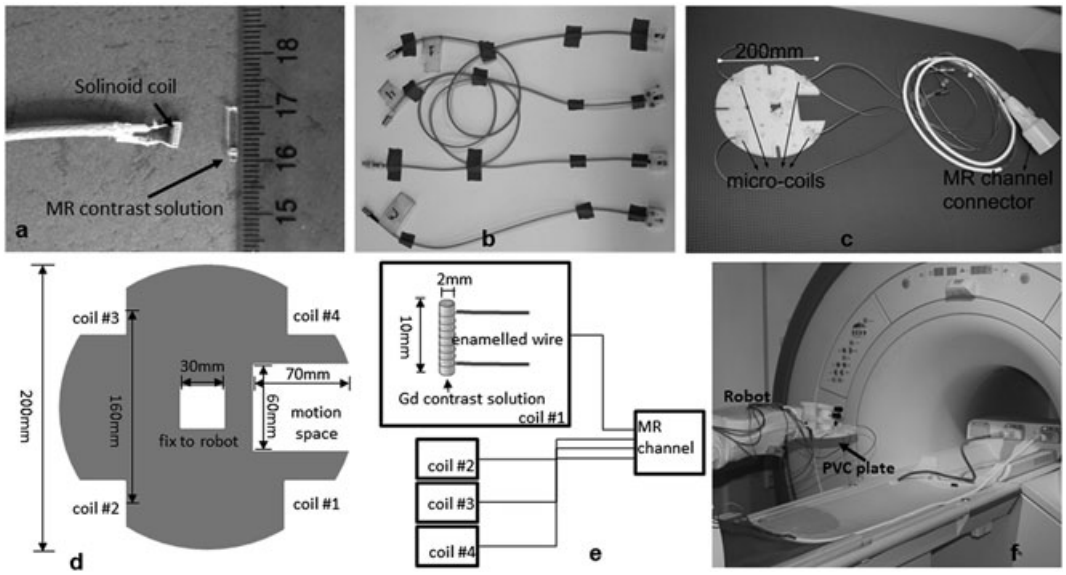

Figure 2. Active tracking hardware: (a) dimension of the micro resonance coils (mRCs) and the container with the gadolinium contrast solution; (b) mRCs with coaxial cable and BNC connector; (c) round PVC tracking plate with four active mRCs; the connector channel is used to connect the mRCs to the MR receiver; (d) diagram of the tracking plate; (e) diagram of the mRCs; (f) fixing the PVA tracking plate onto the robotic arm.

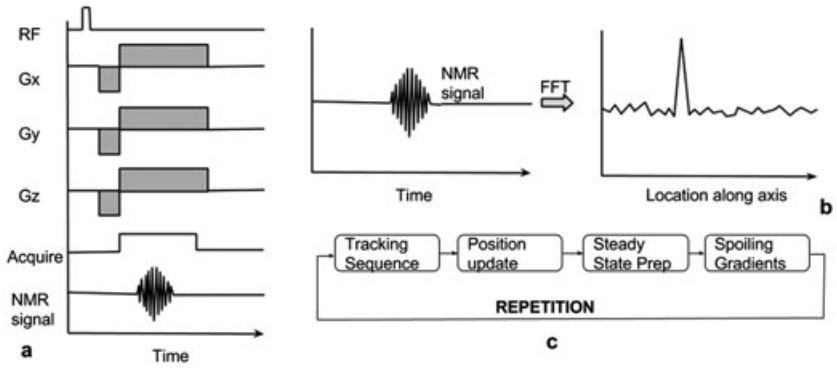

Figure 3. Schematic diagram of pulse sequence for real-time tracking of mRCs with MR as previously proposed (23). Note: phase-field dithering is not shown for simplicity. (a) The pulse sequence employs a non-selective radiofrequency pulse that excites spins within the active volume of the excitation coil. MR data are acquired in the presence of a frequency-encoding gradient. The frequency encoding gradient pulse is multiplexed with a Hadamard scheme as described by Dumoulin *et al.* (19). The polarity [Gx,Gy,Gz] of the frequency-encoding gradient for the four readouts is B1 = [+,+,+], B2 = [−,−,+], B3 = [−,+,−],B4 = [+,−,+]. (b) The position of a signal source (mRC) with respect to an applied magnetic field gradient is determined by Fourier transformation of the MR data, (c) The mRC position is determined by the tracking sequence, which then automatically emits a coordinate update before a steady state stabilization interval. Finally, spoiling gradients are applied to dephase the magnetization, and thus reduce phase coherences before the next repetition.

direction, isotropic tracking resolution = 1.8 mm, slice thickness = 300 mm.

Four mRCs are fixed on a round PVC board with a diameter of 200 mm (Figure 2). A coaxial cable connects the four mRCs, each to an MRI receiver channel for the scanner to acquire MR data, respectively. The PVC board is fabricated as a connector to the robot, and the total weight of the board is about 330 g. The four mRCs are evenly distributed on the edge of the plate and are centrosymmetric to the hole in the centre of the PVC board, which fixes medical devices, e.g. biopsy needle or focused ultrasound transducer.

The minimum number of mRCs to define the position of the robotic arm is three. In this setup we used four; they are axisymmetric to two main motion axes of the robotic arm, which are parallel to the axial axis and sagittal axis of the MR scanner, respectively. The geometrical centre of them is used as the position of the application part of

DOI: 10.1002/rcs

the robotic arm, and the normal vector of the plane is then constructed from the four mRCs and represents the orientation of the application module of the robot (Figure 4), which coincides with the axis of medical devices, e.g. tip of biopsy needle or focus of ultrasound transducer. The position of the robotic arm is marked in a reconstructed 3D MR space, from which the relative relationship between the robotic arm and the target phantom or tissue can be obtained.

The reason we use 4 mRCs is explained by the simulation in Appendix I. We proved that this redundant design using four mRCs is able to compensate the errors more easily than using three if the robotic arm deviates from its expected gesture with respect to the coronal direction. Increasing the number of mRCs to more than four will not distinctly decrease the treatment tool tip distance deviation any further.

Data were communicated between the MRI scanner and an external high performance workstation (Ubuntu 12.04 64bit, 16-CPU, 32 GB memory, Palo Alto, USA) via Ethernet. The pulse sequences were designed in a SpinBench and implemented in RTHawk (24) (HeartVista, Inc., Palo Alto, CA, USA). We used a real-time visualization application Vurtigo (25) (Sunnybrook Health Sciences Centre, Toronto, Canada) to render the mRC position.

Calibration

Before applying the active tracking technique to a FUS treatment guided with the robotic arm, a calibration experiment was required to evaluate the tracking accuracy in a specific range (Figure 5, not in scale). Area

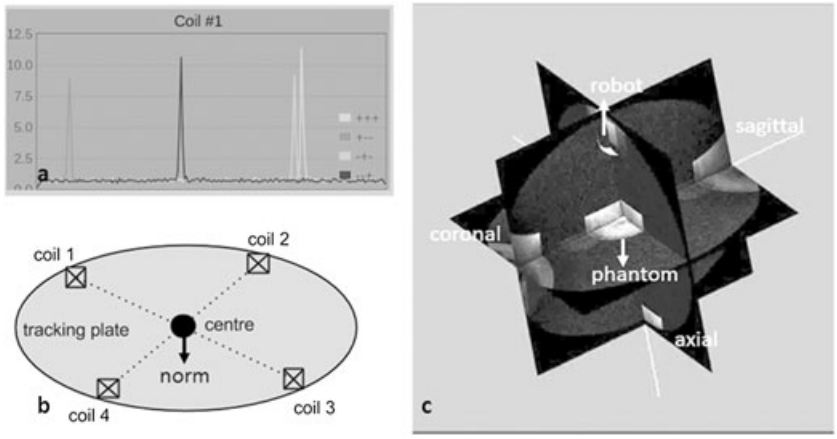

Figure 4. (a) Exemplarily tracking plot for one mRC (No. 1). The four peaks represent the result of the Fourier transform of the MR data. Note that the four colours and peaks represent data that are acquired with the four Hadamard encoded readouts. (b) Structure of the four mRCs; the four coils are distributed evenly on the round plate; (c) reconstructed position of the application module of the robotic arm in a 3D MR space. Three orthogonal MR planes are rendered in 3D MR space, the position and orientation information is also demonstrated.

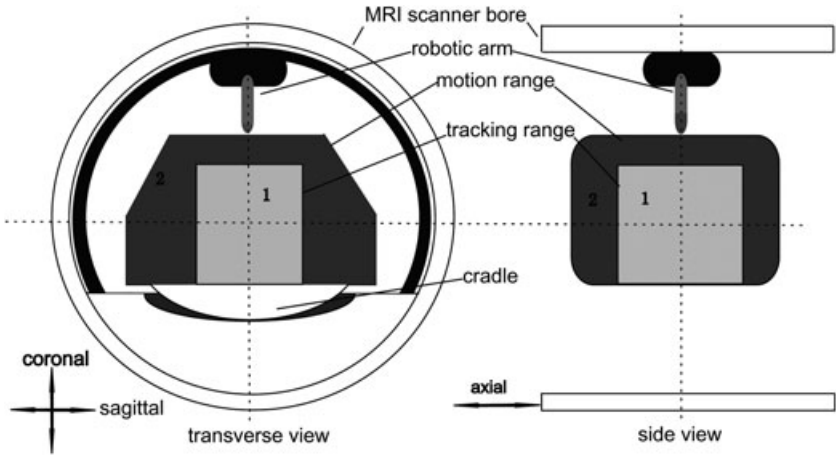

Figure 5. Diagram of MR scanner, robotic arm and its motion range (labeled 2), the tracking experiments were carried out in area 1.

DOI: 10.1002/rcs

2 is the maximum reachable range of the robotic arm. After a rough measurement, it was determined that the application module of the robot can move within a range –170 mm to +170 mm in the sagittal, –80 mm to +100 mm in the coronal and –70 mm to +70 mm in the axial direction at flexible gestures. Active tracking was tested in an area of 160 × 160 × 140 mm (sagittal, coronal and axial directions, respectively. This is labeled 1 in Figure 5.

A 3D reference model (Figure 6) was designed to provide reference points for the test. Reference points were distributed on a phantom made of 5% proportion agar with the size 140 × 140 × 140 mm. The 35 reference holes are located uniformly on seven different layers, the height distance between two adjacent layers is 20 mm and the lateral distance between two adjacent holes is 30 mm. It was found that the 5% proportion agar was stiff enough so that the overall dimension change was negligible for the accuracy study.

To confirm the robotic arm reaching the reference points, a straight needle anchor (Figure 6(b)) was rigidly fixed at the centre of the tracking device. The end of the needle anchor was filled with gadolinium doped gelatine. The described active tracking implementation was used to monitor the robotic arm while guiding the needle anchor to reach all reference points of the phantom on a point by point basis. The tip of the needle anchor appeared brighter than the agar phantom. This enabled the user to confirm its position in MR images (Figure 6 (c), (d)) that were obtained with an interventional coil (DuoFlex, MR Instruments, Hopkins, MN, USA). The MR images (Gradient Echo, TR/TE = 100/30 ms, flip angle = 60°, bandwidth = 31.2 kHz, FOV = 15 × 15 cm, matrix = 512 × 512, slice thickness = 2 mm) served for confirmation of whether the needle anchor was at the correct location or not. In addition, a wireless surveillance web camera (M1011w, Axis, Lund, Sweden) (Figure 7) with 10× zoom lens was used to confirm the position of the robotic arm.

The tracking accuracy at each measured point was determined by comparing the measured positions $\vec{r}_m$ with the theoretical positions $\vec{r}_r$ provided by the reference

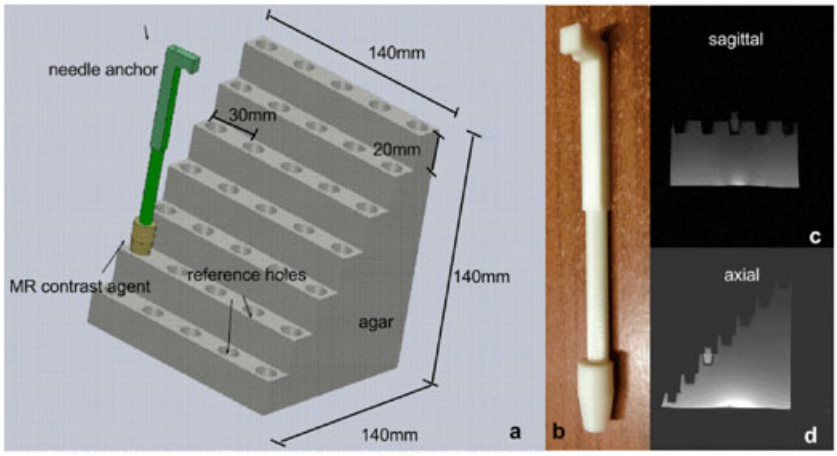

Figure 6. (a) diagram of how the needle anchor located at the reference points of the agar phantom; (b) needle anchor that fits into the reference holes of the phantom, the upper connector was fixed at the applicator module of the robotic arm; (c, d) MR scans to confirm the needle is at the correct position.

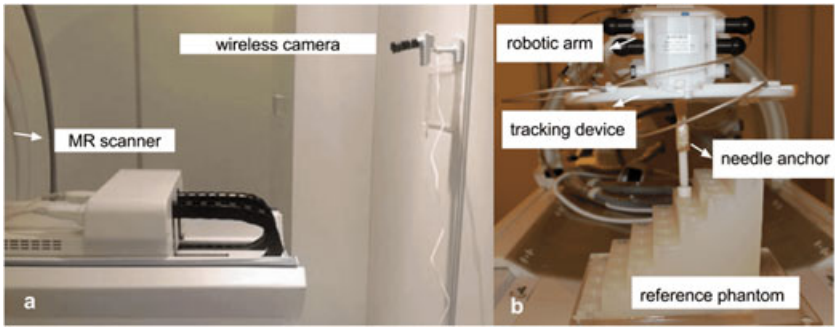

Figure 7. The web camera was used to monitor the needle anchor while it was positioned into the reference holes of the agar phantom as well.

DOI: 10.1002/rcs

phantom on a point-by-point basis as $\vec{\epsilon_i} = \vec{r}_{r_i} - \vec{r}_{m_i}$ (26). Note that all the errors are positive from the equation $|\vec{\epsilon_i}| = |\vec{r}_{r_i} - \vec{r}_{m_i}|$.

Besides the tracking position errors, the orientation errors could be computed by comparing the norm of the plane formed by every group of four active trackers with the coronal direction in the MR bore.

Phantom sonication

A phantom sonication experiment was designed to apply the tracking technique for the robotic arm guided FUS, based on the previous calibration. All the sonications were conducted in a 1.5 T whole body MR scanner (Signa HDxT, GE Healthcare, United States) with a breast Coil (InSightec, Ltd, Tirat Carmel, Israel).

The tracking plate is an exchangeable device, which has a clip for fastening the US transducer (Figure 8). The single element US transducer was fabricated according to MRI compatible requirement (working frequency: 1.09 MHz, focal length: 70 mm, aperture: 60 mm; elliptical –3 dB focus size: ø = 1.8 mm; length = 10 mm, weight: 180 g).

A target egg-white gel phantom (27) with a size of $100 \times 50 \times 50$ mm was used for a specific pattern sonication. The egg-white percentage was 25% in order to make it more transparent for lesions visibility.

The US transducer replaced the needle anchor, so geometrically, the registration of the transducer in the MR reference frame could be done similarly. A breast coil with radius 100 mm was set up as metacoil and used for simultaneous tracking and MRI based thermometry (3). Three phased MR images for thermometry are located near the focus according to the relative distance from the FUS transducer to the centre of the four mRCs. Considering the restriction of the whole setup, the US transducer allows a maximum sonication volume of $5 \times 5 \times 4$ cm^3 to ablate.

A series of sonications was performed with this setup. The targets were distributed with three layers, and the distance between two layers was 10 mm. In the series, two targets were sonicated at the first layer, four targets at the second and sixteen at the third. For each layer, the lesions were parallel to the axial and sagittal direction, and the layered direction was the coronal axis of MRI bore. The robotic arm guides the US transducer to expected position to apply the sonications.

The post-FUS lesions were visually observed and validated by T2-weighted MR scans (FRFSE; TR/TE = 3000/79 ms; FOV = 10 × 10 cm; matrix: 256 × 256; slice thickness = 5 mm; bandwidth = 31.2 kHz). The ablations area was scanned vertically and parallel to the axis of US beam. Then the centroid positions and the sizes of the lesions were calculated using a centre-of-mass algorithm based on the MR images at a sub-pixel level to evaluate the positioning performance of the active tracking assisted FUS system.

Results

Calibration results

The distance error distribution for the centre of four mRCs is plotted as a frequency histogram (Figure 9).

In the measurement range $160 \times 160 \times 140$ mm (Figure 5), the overall RMS distance error is 0.43 mm (labeled B in Figure 9). Most of the errors lie within twice the actual RMS, with maximum error of 2.74 mm (labeled D in Figure 9) being an order of magnitude greater than the RMS. Errors larger than 1.50 mm occurred at the boundary of the measurement range, and were spotted only six times out of a total measuring number of 149.

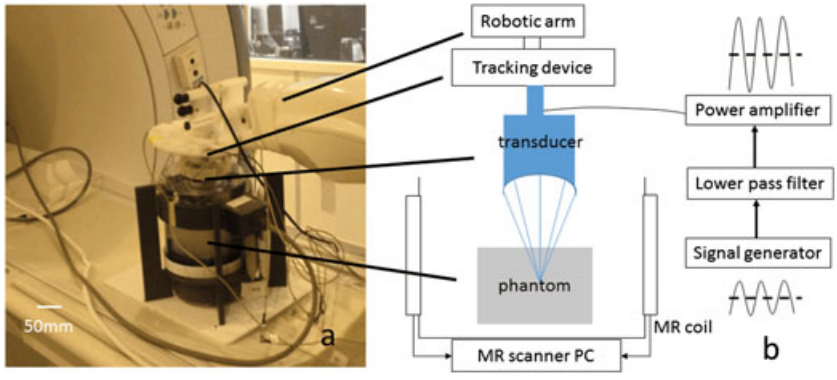

Figure 8. Schematic diagram and photo of the robotic arm used to guide the FUS transducer for sonications. From top to bottom are the robotic arm, the tracking plate, the FUS transducer, the breast coil, and the egg-white gel phantom. The FUS transducer was placed into degassed water to couple with the target phantom.

DOI: 10.1002/rcs

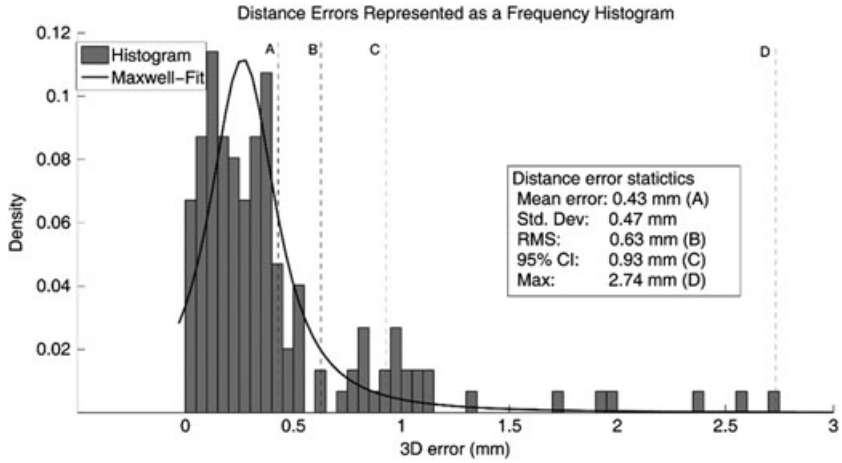

Figure 9. Frequency histogram of the distance errors for the centre of four mRCs. The distribution is roughly estimated to a Maxwell probability distribution. A distance error statistical summary is listed including the root-mean-square (RMS), the bias (mean error), its spread (standard deviation), maximum error and 95% confidence interval (CI), which are labelled in the histogram.

When the measurement range was reduced to $150 \times 150 \times 140$ mm, the maximum error was smaller than 1.5 mm. To avoid damaging healthy tissues, these positions were not considered when the robotic arm was to be used to guide a FUS transducer to sonicate a target. The mean error and standard deviation are 0.43 mm and 0.47 mm, respectively (labeled A in Figure 9).

The Maxwell distribution curve fits similarly but not completely to the data (26). Figure 9 shows that the errors in the coronal direction play a more important role than the other directions for the distance errors. In the coronal direction, the RMS is 0.57 mm, and in the axial and coronal, the RMS is 0.14 mm and 0.23 mm, respectively. This implies that the distance errors have dependence on coronal direction, which is not completely in conformity with the Maxwell probability distribution. The gross systematic errors in the coronal direction are due to the weight of the tracking plate, which is much heavier than a biopsy needle. An estimation can be made that the error in the coronal direction was two times larger than in the other two directions (Figure 10). However, the Maxwell fit could give us a brief idea of the errors distribution, as the confidence interval indicates that 95% errors are restricted, which is smaller than 0.93 mm (labeled C in Figure 9).

The results of the distance errors for each mRC, as well as the average results are shown in Table 1. Compared with Figure 9, the distance errors for the application module of the robotic arm are slightly, yet significantly, better than the single mRC results, which is a consequence of the inherent averaging of the mRC errors during the calculation of the centres from the underlying mRC positions.

Since the four markers theoretically constructed a rigid body, the orientation errors are calculated by comparing the norm of the tracking plate, which fitted from the coordinates of four mRCs with the coronal direction vector of the MRI bore. The bias of orientation errors is 0.31° (mean) or 0.36° (median) with a standard deviation of $\pm 0.15°$. 95% of orientation errors are smaller than 0.50°.

To summarise, the active tracking was calibrated over the whole measurement area ($140 \times 160 \times 180$ cubic mm,

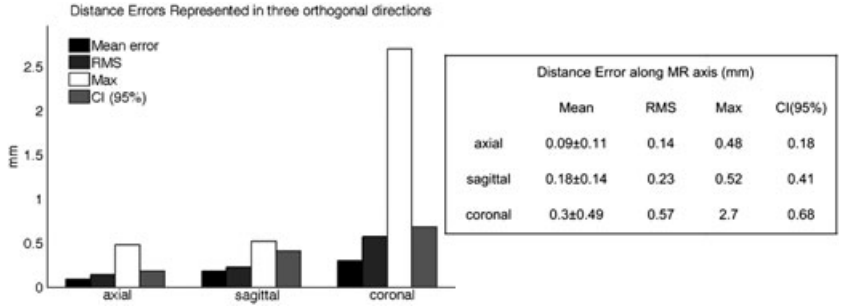

Figure 10. Distance error bars in three orthogonal directions for the centre of four mRCs. The distance errors are positive. The statistical summary contains the bias and standard deviation, maximum error and 95% confidence interval.

DOI: 10.1002/rcs

Table 1 Single marker accuracies for the individual mRC, as well as their averaged results

Marker	RMS (mm)	Mean (mm)	Std. Dev. (mm)	Max (mm)	95% CI (mm)
mRC #1	0.80	0.54	0.60	3.24	1.15
mRC #2	0.78	0.50	0.59	3.44	0.99
mRC #3	0.68	0.50	0.47	2.79	0.96
mRC #4	0.73	0.53	0.51	2.68	1.07
Average	0.75	0.52	0.54	3.04	1.04

Figure 5). The distance errors for the centres of four mRCs are presented with RMS = 0.63 mm as well as the 95% confidence interval with 0.93 mm. The distance errors are greater in the coronal direction than in the other directions. To some extent, the orientation errors of the setup show a bias, and its spread, as $0.31 \pm 0.15°$.

What is more, the tracking was repeated over 20 times at each reference position, and the deviation was around 0.07 mm over the whole calibration area, which indicated a high robustness of this method.

Ablation results

During all ablations, the temperature at the foci was monitored by MR thermometry in real time. With the same ultrasound protocol (sonication duration: 25 s; acoustic intensity: $800\,W \cdot cm^{-2}$; power efficiency was measured by force balance, area of focus was scanned by needle hydrophone), an average temperature of 55 °C was reached at the ultrasound foci, which was sufficient to cause protein denaturation in the egg-white gel phantom.

Photographs of the egg-white phantom corresponding to the MR images were taken after the ablation (Figure 11). Since the sonication pattern was with a 3-layer structure, some of the photographs were taken after the phantom had been sliced in order to observe the inner layout of the lesions. The lesions in the phantom were scanned in two directions – one perpendicular to the axis of the US beam and the other parallel to it.

The results of the phantom ablation experiments are summarised (Table 2) to evaluate the applicability of the active tracking assisted robotic arm setup, in which the accuracy of the lesion positions as well as the lesion dimensions are demonstrated. The distance errors between the calculated centre of the lesion and the theoretical position recorded from the mRCs were $\Delta x = 0.4 \pm 0.37$ mm, $\Delta y = 0.4 \pm 0.28$ mm and $\Delta z = 0.7 \pm 0.66$ mm, respectively, in the coordinate system of the application module on the robot, where the x, y directions were vertical to the axis of the US beam; z direction was along the US beam. The z direction was along the layered direction parallel to the coronal direction of the MRI bore. We found that the distance errors of the lesions in the z direction were greater than in the other two directions, which might be because that the length of the lesions varied more when the MR scan plane was mal-positioned from the axis of the lesions.

The error for the active tracking was not considered because the readout from the mRCs was taken as the theoretical positions of the robotic arm. The deviation of active tracking was 0.01 mm, which means there was a small fluctuation during the monitoring process of the robotic arm. The deviation value was calculated by repeating 20 measurements for every ablation position. It was assumed to increase if the focal scanning volume became large.

Discussion

In this work, a combination of a commercial available robotic arm, a bowel-shaped fixed single focus FUS transducer and a customised active tracking device was proposed for MRgFUS therapy. The active tracking implementation was calibrated and a series of phantom ablation experiments was conducted, from which the localisation accuracy and applicability for MRgFUS of this combined setup were assessed.

An application based on RTHawk communicated with the GE MR scanner in real time and the coordinates of the robotic arm were monitored and recorded. Furthermore, the position and gesture of the robotic arm were reconstructed in a virtual 3D space where the phantom/tissue position was also included. With in-house developed software, the active tracking obtained the device position within 120 milliseconds. By employing a three phased dithering direction rather than six, the tracking time decreased to 60 milliseconds, which satisfies tracking applications in a smaller volume.

As mentioned above in the calibration experiment, the tracking distance errors in the coronal direction were generally greater than the errors in the other two directions (Figure 10). In the coronal direction, the RMS is 0.57 mm, and in the axial and coronal, the RMS is 0.14 mm and 0.23 mm, respectively. Because the robotic arm was designed to guide needle biopsy, the weight of the tracking plate is around 333 g, which is much heavier than a biopsy needle. The heavier plate might cause bending in the robotic arm when the robotic arm moves, which brings the systematic error. Also, according to the calculation in Appendix I, the design that the four mRCs are in the same plane makes the tracking more vulnerable in coronal direction than in the other directions since the

DOI: 10.1002/rcs

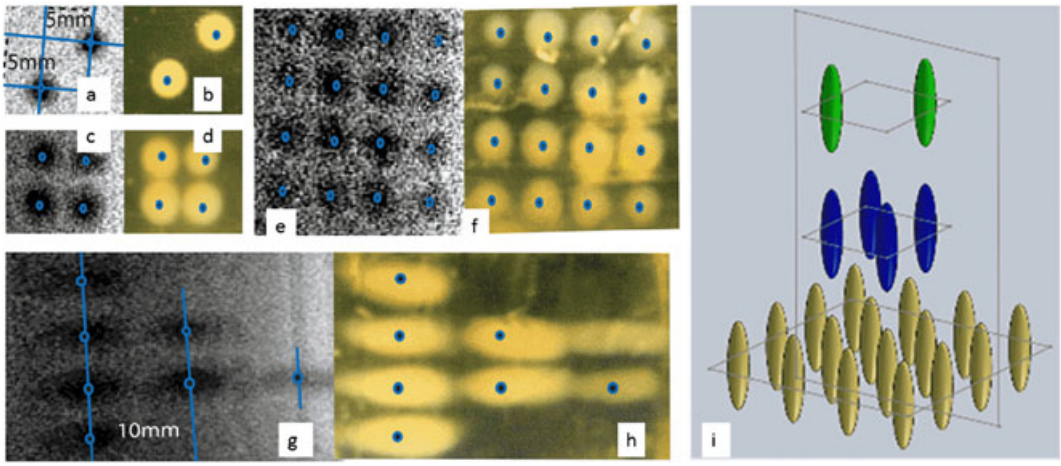

Figure 11. Photographs (a, c, e, g) of the lesions and corresponding enlarged section of post-FUS MR scans (b, d, f, h) after image enhancement using ImageJ. Some of the lesions in the photograph did not match the MR images exactly because the slicing position of the phantom did not coincide with the corresponding MR scan position. The lesions were distributed in a 3-layer square pattern (i); the target points were distributed in a square shape in every layer, and the two targets at the top layer occupy the two corners of a square.

Table 2 Results of the phantom ablation experiments for the setup. Δz is the distance error in the US beam axis direction, approximately parallel to the coronal direction of the MR scanner; Δx and Δy are the distance errors in the direction perpendicular to the US beam axis; d_{rad} and l are the minor and major diameter of the elliptic lesions in the side view

Measurements based on MR images (mm)				
Δx	Δy	Δz	d_{rad}	l
0.4 ± 0.37	0.4 ± 0.28	0.7 ± 0.66	3.0 ± 0.18	6.0 ± 0.36

norm of the plane is parallel to the coronal axis. However, the strength of this design is that the tracking plate allows adequate space to fix medical devices, e.g. biopsy needles or FUS transducers. And the axes of the medical devices coincide with the axis of the tracking plate, which makes the medical treatment plan easy to implement. If higher and uniform tracking accuracy is needed, the suggestion would be to change the distribution of the mRCs from four corners of a plane to four endpoints of a tetrahedron or other isotropic shapes.

Besides the orientation dependence, the distance errors were found to increase when the mRCs were far from the iso-centre because of magnetic gradient inhomogeneities (28). Thus, the design using multiple coils to construct a rigid body is preferable to using a single marker since the distance errors were eliminated to a certain extent by averaging the tracking results from the groups of markers.

The application module of the robotic arm could reach an FOV of about 50 cm × 50 cm, yet the active tracking was not calibrated over the whole spatial range. Because the receiving coil has a size of 10 cm × 10 cm, the calibration experiment had only evaluated the active tracking techniques over an acceptable spatial range of 160 mm × 160 mm × 140 mm (sagittal, axial and coronal directions, respectively). In this range, the robotic arm has to reach some limited positions of the FOV in an extremely oblique gesture. This made it difficult to insert the needle anchor into the reference holes of the gel phantom because the trajectory of the insertion operation is unpredictable at these limited positions. If these limit positions are neglected, the guiding precision of the robotic arm was better than 1.5 mm. By employing a larger receiving coil, a larger range could be calibrated similarly.

A passive marker is characterised by various imaging or post-processing methods (16). Our presented active tracking is competitive with a passive marker. Most of the errors are distributed smaller than 1 mm for both methods. It is difficult to compare them directly since their results were mostly described using mean and deviation. But for the positive distance errors, which in theory are not a normal distribution, we prefer to use RMS and confidence intervals such as 90% or 95% to describe the result. RMS error has the advantage of incorporating both the trueness and precision in a single value as $\approx\sqrt{\mu^2+\sigma^2}$. Confidence intervals indicate the results better when there are larger errors in the distribution tails, which could be easily omitted if using deviation for describing them.

Based on the active tracking guidance, the robotic arm moved an MR-compatible single element HIFU transducer to finish an ablation pattern in egg-white gel phantom. Compared with the errors using passive tracking for the same robotic arm to guide sonication in a phantom (29), which is 0.5 ± 0.4 mm and 0.9 ± 0.6 mm vertical and

DOI: 10.1002/rcs

parallel to the coronal direction in the MRI bore, the final lesion location distance errors using active tracking had similar performance.

The lesion location distance errors ($\Delta x = 0.4 \pm 0.37$ mm, $\Delta y = 0.4 \pm 0.28$ mm and $\Delta z = 0.7 \pm 0.66$ mm, Table 2) are slightly larger than the tracking distance errors ($\Delta x = 0.09 \pm 0.11$ mm, $\Delta y = 0.18 \pm 0.14$ mm and $\Delta z = 0.3 \pm 0.49$ mm, Figure 10) in the relative direction. The larger distance errors along the z (coronal) dimension come from tracking errors. The four mRCs were designed to be distributed at a same plane. This design made the tracking accuracy more vulnerable to errors in the z dimension (perpendicular to the plane) than the other two dimensions (axial and sagittal). More mRCS or a stereoscopic distribution design might help to decrease the errors. However, the experiment result is comparable with Dorian *et al*. who achieved an accuracy of $\Delta x = 0.4 \pm 1.0$ mm, $\Delta y = 0.5 \pm 2.4$ mm and $\Delta z = 0.7 \pm 1.2$ mm in the heads of fresh cadavers using an MR guided phased-array FUS transducer (30). Considering the voxel size of the MRI sequence $0.4 \times 0.4 \times 5$ mm(3), we could conclude that the location of these lesions was precisely reached via this mechanical guidance method.

By investigating the MR scans and photographs of the post-FUS phantoms, the sizes of the lesions varied a little, which demonstrates the influence of the different US absorptions in different areas of the phantom. The shapes of the lesions were also different from the theoretic shape of the acoustic focus of the characterised US transducer. When applying the method *in vivo*, a lower power of focused ultrasound should be considered for safety reasons. Considering that the lesions were with diameters of around 3 mm and lengths of about 6 mm (Table 2), the precision of focal relocation was sufficient for focal scanning large tumours.

For MRgFUS, it is difficult to conduct manual relocation of the FUS transducer because of the space limitation of the MR bore. Manual repositioning of the FUS transducer is generally used in ultrasound guided focused ultrasound surgery (USgFUS). Researchers (31) achieved a distance of 1.3 ± 2.0 mm from the expected position of lesions via manual fixation of the FUS transducer in their *in vivo* USgFUS treatments. The FUS zones had an average diameter of 15.3 ± 2.3 mm and an average depth of 15.5 ± 3.1 mm. By contrast, MRgFUS using mechanical relocation of the transducer has smaller errors than USgFUS by manual relocation.

If the setup needs to be tested on human or animal tissues, a new treatment unit should be developed to allow the transducer to cling on the skin surface. The US transducer should be embedded in a water-filled bellows, which could be fixed onto the skin via stretchable straps (29). To our knowledge, the ExAblate 2100 system (InSightec, Ltd, Tirat Carmel, Israel) uses a strong membrane that restricts degassed water within the treatment range to fit onto skin surface. This FUS setup might introduce a systematic localisation error since the water-bellows on the skin surface will make the tissues deform in the direction of pressure. Since our ablation experiments mainly focused on evaluating the active tracking techniques for a robotic arm assisted MRgFUS, only degassed water was used for coupling the US transducer to the phantom to avoid non-necessary deformations. However, by designing a new treatment unit with a water-bellow, the setup could be applied for animal or human tissue ablations.

The active tracking sequence and thermometry sequence could alternate between each other to enable real-time localisation of the device and treatment monitoring (32). This implementation allows the combined robotic system to quickly adjust the US focus even during sonication because both the active tracking and MR thermometry scans are not very time consuming.

The combination of this active tracking assisted robotic system and the ExAblate 2100 system is fascinating. This might make the most of the large operational range of the robotic arm with active tracking and flexible treatment access of the portable US transducer. Furthermore, after combining the relatively slow focal scanning of the robotic arm and the fast beam-steering of the phased-array US transducer, the problems caused by a patient's involuntary motion can be resolved. The robotic arm will relocate the US transducer if the patient motion exceeds a certain range, and the phased-array US transducer will steer the focus electronically if the movements are too fast for mechanical relocation.

To conclude, active tracking was developed to monitor the position of a robotic arm with an acceptable accuracy at sub-second update rates. The integration of the active tracking technique and robotics has the potential to guide a FUS transducer to deliver ablations. With the in-house developed software, US focus repositioning can be controlled with an accuracy of better than 1.5 mm. The calibration of active tracking and phantom ablation experiments assessed the feasibility of this combined system for MRgFUS, which made this setup competitive with the beam-steering technique of phased array FUS.

Acknowledgements

The authors would like to thank Vladimir Olsan (Senior Design Consultant, IBSMM Engineering spol. s. r.o./Ltd., Czech Republic) for his support in developing robotic arm controlling software, and hardware maintenance. The authors thank Zhen Qiu (Division of Imaging and Technology, University of Dundee, Dundee, UK) for her

DOI: 10.1002/rcs

help on the fabrication and characterisation of the MR-compatible US transducer and for help during the phantom ablation experiment. The authors thank Alexander Volovick (InSightec, Ltd, Tirat Carmel, Israel) for his suggestions on the design of the tracking device. The China Scholarship Council (CSC) is thanked for the financial support of this work. The research leading to these results has also received funding from the European Union's Seventh Framework Programme under grant agreement no. 270186 (FUSIMO project) and no. 611963 (FUTURA project).

Conflicts of interest

Xu Xiao, Martin Alexander Rube, Dr. Zhihong Huang, and Professor Andreas Melzer declare that they have no conflicts of interest for this work.

Ethics

Approval by an ethics committee was not applicable for this work. Statement of informed consent was not applicable since the manuscript does not contain any patient data.

Appendix I

Assume the 4 micro resonance coils (mRCs) are in a theoretically plane, ideally their coordinates are $A_1(0, 0, 0)$, $A_2(0, 160, 0)$, $A_3(160, 0, 0)$, $A_4(160, 160, 0)$. Then the plane is $z = 0$. And the normal vector of the plane is

$$\hat{n} = (0,\ 0,\ 1)$$

If in the tracking, A_1 is measured with an error of 1.0 mm in z direction, which leads to the new coordinates $A_{1e}(0, 0, 1)$. Let us ignore A_4, the points A_{1e}, A_2, A_3 can determine the calculated plane which is with a normal vector of $\hat{n}_1 = (0.0062,\ 0.0062,\ 1.0000)$. So the angle between the calculated plane and the theoretical plane is $\alpha(\hat{n}, \hat{n}_1) = \cos^{-1}(\hat{n} \cdot \hat{n}_1) = 0.0088$.

Considering the treatment tool tip (the focus of the intensity ultrasound transducer) is 80 mm far from the plane, this measurement error of mRC will eventually result in a treatment tool tip distance deviation

$$d_1 = 80 \times \alpha(\hat{n}, \hat{n}_1) = 0.7071\ mm.$$

However, if we take account of four points. The points A_{1e}, A_2, A_3, A_4 could fit (1) to a plane with a normal vector of $\hat{n}_2 = (0.0031,\ 0.0031,\ 1.0000)$. So the angle between the calculated plane and the theoretical plane is

$$\alpha(\hat{n}, \hat{n}_2) = \cos^{-1}(\hat{n} \cdot \hat{n}_2) = 0.0044$$

Thus the treatment tool tip distance deviation will be $d_2 = 80 \times \alpha(\hat{n}, \hat{n}_2) = 0.3536$ mm, which is a half of the error when we use 3 mRCs. Thus, if we fix a FUS transducer to the tracking plate, it is better to use 4 mRCs than to use only 3 mRCs to reduce the deviation of the focus of the ultrasound.

References

1. ter Haar G, Coussios C. High intensity focused ultrasound: physical principles and devices. *Int J Hyperth* 2007; **23**(2): 89–104.
2. Jolesz FA, McDannold N. Current status and future potential of MRI-guided focused ultrasound surgery. *J Magn Reson Imaging* [Internet]. Wiley Subscription Services, Inc., A Wiley Company; 2008; **27**(2): 391–399.
3. Rieke V, Butts Pauly K. MR thermometry. *J Magn Reson Imaging* [Internet]. Wiley Subscription Services, Inc., A Wiley Company; 2008; **27**(2): 376–390.
4. Bohris C, Jenne JW, Rastert R, *et al*. MR monitoring of focused ultrasound surgery in a breast tissue model *in vivo*. *Magn Reson Imaging* [Internet]. 2001; **19**(2): 167–175.
5. Tempany CMC, Stewart EA, McDannold N, *et al*. MR Imaging–guided focused ultrasound surgery of uterine leiomyomas: a feasibility study 1. *Radiology* [Internet]. 2003; **226**(3): 897–905.
6. Catane R, Beck A, Inbar Y, *et al*. MR-guided focused ultrasound surgery (MRgFUS) for the palliation of pain in patients with bone metastases – preliminary clinical experience. *Ann Oncol* [Internet]. 2007; **18**(1): 163–167.
7. Ram Z, Cohen ZR, Harnof S, *et al*. Magnetic resonance imaging-guided, high-intensity focused ultrasound for brain tumor therapy. *Neurosurgery* [Internet]. 2006; **59**(5): 949–956 10.1227/01.NEU.0000254439.02736.D8.
8. Hynynen K, Clement G. Clinical applications of focused ultrasound – the brain. *Int J Hyperth* [Internet]. 2007/06/21 ed. 2007; **23**(2): 193–202.
9. McDannold N, Clement GT, Black P, *et al*. Transcranial magnetic resonance imaging- guided focused ultrasound surgery of brain tumors: initial findings in 3 patients. *Neurosurgery* [Internet]. 2010/01/21 ed. 2010; **66**(2): 323–332; discussion 332.
10. Furusawa H, Namba K, Nakahara H, *et al*. The evolving non-surgical ablation of breast cancer: MR guided focused ultrasound (MRgFUS). *Breast Cancer* [Internet]. 2007/01/25 ed. 2007; **14**(1): 55–58.
11. Melzer A, Gutmann B, Remmele T, *et al.* INNOMOTION for percutaneous image-guided interventions. *Ieee Eng Med Biol Mag* 2008; **27**(3): 66–73.
12. Patil S, Bieri O, Jhooti P, Scheffler K. Automatic slice positioning (ASP) for passive real-time tracking of interventional devices using projection-reconstruction imaging with echo-dephasing (PRIDE). *Magn Reson Med* [Internet]. 2009/07/09 ed. 2009; **62**(4): 935–942.
13. de Oliveira A, Rauschenberg J, Beyersdorff D, *et al*. Automatic passive tracking of an endorectal prostate biopsy device using phase-only cross-correlation. *Magn Reson Med* [Internet]. 2008/04/23 ed. 2008; **59**(5): 1043–1050.
14. Konings MK, Bartels LW, Smits HF, Bakker CJ. Heating around intravascular guidewires by resonating RF waves. *J Magn Reson Imaging* [Internet]. 2000/08/10 ed. 2000; **12**(1): 79–85.

15. Rea M, McRobbie D, Elhawary H, *et al*. Sub-pixel localisation of passive micro-coil fiducial markers in interventional MRI. *MAGMA* [Internet]. 2008/09/20 ed. 2009; **22**(2): 71–76.
16. Flask C, Elgort D, Wong E, *et al*. A method for fast 3D tracking using tuned fiducial markers and a limited projection reconstruction FISP (LPR-FISP) sequence. *J Magn Reson Imaging* [Internet]. 2001/12/18 ed. 2001; **14**(5): 617–627.
17. Thormer G, Garnov N, Moche M, *et al*. Simultaneous 3D localization of multiple MR-visible markers in fully reconstructed MR images: proof-of-concept for subsecond position tracking. *Magn Reson Imaging* [Internet]. 2012/01/17 ed. 2012; **30**(3): 371–381.
18. Rube MA, Holbrook AB, Cox BF, *et al*. Wireless MR tracking of interventional devices using phase-field dithering and projection reconstruction. *Magn Reson Imaging* [Internet]. 2014; **32**(6): 693–701.
19. Dumoulin CL, Souza SP, Darrow RD. Real-time position monitoring of invasive devices using magnetic resonance. *Magn Reson Med* [Internet]. Wiley Subscription Services, Inc., A Wiley Company; 1993; **29**(3): 411–415.
20. Weiss Luedeke KM S, Leussler C, *et al.* Catheter localization using a resonant fiducial marker during interactive MR fluoroscopy. *Int Soc Magn Reson Med* 1999; **7**: 1954.
21. Cleary K, Melzer A, Watson V, *et al*. Interventional robotic systems: applications and technology state-of-the-art. *Minim Invasive Ther Allied Technol* [Internet]. 2006/06/07 ed. 2006; **15**(2): 101–113.
22. Burl M, Coutts GA, Young IR. Tuned fiducial markers to identify body locations with minimal perturbation of tissue magnetization. *Magn Reson Med* [Internet]. Wiley Subscription Services, Inc., A Wiley Company; 1996; **36**(3): 491–493.
23. Dumoulin CL, Mallozzi RP, Darrow RD, Schmidt EJ. Phase-field dithering for active catheter tracking. *Magn Reson Med* [Internet]. 2010/05/01 ed. 2010; **63**(5): 1398–1403.
24. Santos JM, Wright GA, Pauly JM. Flexible real-time magnetic resonance imaging framework. In *Engineering in Medicine and Biology Society*, 2004 IEMBS '04 26th Annual International Conference of the IEEE. 2004. 1048–1051.
25. Radau PE, Pintilie S, Flor R, *et al*. VURTIGO: Visualization Platform for Real-Time, MRI-Guided Cardiac Electroanatomic Mapping. In: Camara O, Konukoglu E, Pop M, Rhode K, Sermesant M, Young A, editors. *Statistical Atlases and Computational Models of the Heart Imaging and Modelling Challenges: Second International Workshop, STACOM 2011, Held in Conjunction with MICCAI 2011, Toronto, ON, Canada*, September 22, 2011, Revised Selected Papers [Internet]. Berlin, Heidelberg: Springer Berlin Heidelberg; 2012. p. 244–53.
26. Wiles AD, Thompson DG, Frantz DD. Accuracy assessment and interpretation for optical tracking systems. In *Medical Imaging 2004: Visualization, Image-Guided Procedures, and Display*. Proc. SPIE 5367: San Diego, CA, 2004; 421–432.
27. Gao J, You J, Huang Z, et al. Simultaneous measurement of thermophysical properties of tissue-mimicking phantoms for high intensity focused ultrasound (HIFU) exposures. *Int J Thermophys* [Internet]. Springer US; 2012; **33**(3): 495–504.
28. Kuhl CK, Kooijman H, Gieseke J, Schild HH. Effect of B1 inhomogeneity on breast MR imaging at 3.0 T. *Radiology* [Internet]. 2007/08/22 ed. 2007; **244**(3): 929–930.
29. Krafft AJ, Jenne JW, Maier F, *et al*. A long arm for ultrasound: a combined robotic focused ultrasound setup for magnetic resonance-guided focused ultrasound surgery. *Med Phys* [Internet]. AAPM; 2010; **37**(5): 2380–2393.
30. Dorian Chauvet, Laurent Marsac, Mathieu Pernot, *et al*. Targeting accuracy of transcranial magnetic resonance–guided high-intensity focused ultrasound brain therapy: a fresh cadaver model. *J Neurosurg* [Internet]. 2013; **118**(5): 1046–1052.
31. Djin WAN, Melodelima D, Parmentier H, Rivoire M, Chapelon JY. *In vivo* preclinical evaluation of the accuracy of toroidal-shaped HIFU treatments using a tumor-mimic model. *Phys Med Biol* [Internet]. 2010; **55**(8): 2137.
32. Andrew B. Holbrook, Andreas Melzer, Kim Butts Paudy MAR. Interventional MRI from the Internet Browser. In 9th Interventional MRI Symposium. Boston, MA; 2012.

DOI: 10.1002/rcs